

Research Paper

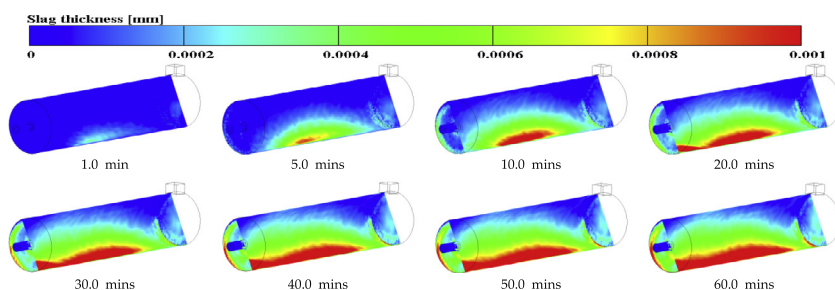
Development of 3D transient wall filming mechanism during combustion by coupling Eulerian-Lagrangian approach and particle-wall interaction model

Arafat A. Bhuiyan ^{a,b}, Jamal Naser ^{a,*}^a Faculty of Science, Engineering and Technology (FSET), Swinburne University of Technology, Victoria 3122, Australia^b Department of Mechanical and Chemical Engineering, Islamic University of Technology (IUT), Gazipur 1704, Bangladesh

HIGHLIGHTS

- A wall filming mechanism was developed during combustion process in small furnace.
- The deposited film on the wall was found to be in good agreement with the available data.
- Slightly higher fraction of film was deposited in oxy-firing due to lower char oxidation rate.
- The deposited film thicknesses on the furnace wall were found in the range of 0–1.0 mm.
- The average molten film flows slowly due to higher viscous and surface tension properties.

GRAPHICAL ABSTRACT



ARTICLE INFO

Article history:

Received 16 June 2016

Revised 24 October 2016

Accepted 27 October 2016

Available online 29 October 2016

Keywords:

Combustion

Oxy-fuel

Slagging

Entrainment

Film thickness

ABSTRACT

In the present study, the developments of 3D wall filming mechanism for coal combustion in a small scale furnace under air and oxy-fuel combustion conditions are presented. The principle objective of this study is to develop the film flow behavior and particle deposition characteristics on the furnace refractory wall using a commercial CFD code coupled with some user-defined sub-routines. Eulerian-Lagrangian approach of the gas-particle flow is coupled with the particle-wall interaction mechanisms including particle capturing, entrainment and wall burning sub-models. A case study has been presented to validate the model in a small scale furnace by comparing the available temperature, species data for coal-water slurry combustion and reasonable agreement has been observed. Visualization of the transient film formation and flow characteristics under air and oxy-firing cases are presented. The film thickness deposited on the refractory wall was found to be reasonably in good range with the available data. The deposited film thicknesses for both the conditions are found in the range of 0–1.0 mm. The average molten film velocity was 0.0001 m/s due to higher viscosity and greater surface tension properties. Slightly higher amount of films are formed in oxy-firing condition due to slower char oxidation rate.

© 2016 Elsevier Ltd. All rights reserved.

1. Introduction

Slagging is a process of combustion in which ash/char particles are heated at a temperature above the fusion temperature, and then becomes molten and thus deposited along the furnace

* Corresponding author.

E-mail address: jnaser@swin.edu.au (J. Naser).

refractory wall. These molten particles form a layer of film called slag [1,2]. Formation of wall film is accountable for the decrease in the disposing of unused mineral content in the environment, reduced energy efficiency, broader fuel flexibility and higher percentage of low-carbon content slag residues for applications [3,4]. Also, the deposited layer of film works as a coating for the prevention of heat loss in the gasifiers. But, it reduces the overall efficiency of the plant. In order to allow slagging combustion, it is important to sustain an optimum state which requires comprehensive information about the related process and mechanisms.

In last two decades, many numerical efforts have been demonstrated for the development of coal and biomass combustion [5–9]. Only few studies were concentrated for slagging combustion [10–15]. Seggiani [16] developed a simplified model for the simulation of time varying slag flow in an entrained flow reactor. In modelling the slag formation, different physical properties such as critical viscosity, specific heat, thermal conductivity were taken into account. This 1D slag model of Seggiani [16] considered Reid and Cohen assumptions [17] and integrated with a 3D code to obtain mass deposition rate, gas temperature and heat flux. Temperature of critical viscosity is considered as an important parameter which is dependent on the composition of slag. Later, Wang [15,18] conducted another steady state model to determine the deposition and burning characteristics during firing of coal and wood. In this model, Particle impingement and particle sticking characteristics are applied by using Wood's [19] and Walsh's [20] mechanisms. The specialty of this model is the wall burning and slag flow process, but only limited for molten slag modelling. Compared to Seggiani's model [16], this Wang model reflects the wall burning phenomenon when fuel particles are stuck on the slag surface and its consequence on char oxidation and heat transfer performance. But both of the model cannot determine the slag behavior in others direction. Yong [21,22] developed a steady state model to describe the flow and heat transfer characteristics in slag layer of solid fuel gasification by combining the model developed by Seggiani [16] and Wang [15,18] as described earlier. In this modelling, an updated temperature profile is assumed replacing Seggiani's assumptions [16]. Bockelie [23] and Chen [24] extended the 1D slag model into the 2D wall surface in fuel combustor. But slag flow is considered in one direction only. This 2D method considers the spatial distribution of ash particle deposition. This approach cannot completely solve the 3D flow behavior. Liu and Hao [25] modeled a two dimensional slag flow in an entrained flow gasifier using the volume-of-fluid (VOF) model. Ni [12] used the same technique to model the multiphase multilayer slag flow and phase transformation considering two-dimensional mesh with uniform ash deposition rate.

Most of the above studies on modelling of slagging are based on 1D and 2D modelling. Only few studies attempted for 3D modelling. Chen [26] developed a comprehensive slag flow model to determine the slag behavior during coal combustion and gasification in a 5 MW pressurized combustor. This model integrated different models for fluid and particle trajectories modelling implemented in a commercial CFD code. This model completely decides the 3D features of char/ash deposition, slag flow, as well as heat transfer through the slag layer. The result showed that 1–2 mm slag layer is formed on the refractory wall which is basically molten. The mean slag flow rate is normally about 0.1 mm/s. The relationship between the slag thickness and slag velocity, heat flux and slag temperature are presented in the numerical work of [15]. It is observed that slag velocity decreases with the increase of slag thickness. Similar trend is observed in the study of Chen [26].

As modelling of wall filming during coal combustion has shown limited progress in the literature compared to other conventional combustion processes [2], hence, the foremost goal of the present study is to develop a comprehensive 3D wall filming mechanism

considering particle capturing, entrainment and wall burning sub-model in a small scale furnace using CFD technique. Also, to examine the factors associated with the particles deposition characteristics that experience between combustion and wall filming-called film wall interactions are important. In order to validate the model, a 5 MWth coal water slurry furnace under air and oxy-firing conditions is considered to identify the filming behavior and related combustion issues. Also, this study looks at the effects of different species level (O_2 , CO_2 , H_2O , CO) and thermal and flow behavior under selected conditions using a commercial CFD code coupled with required user-defined subroutines.

2. Development of the model

An understanding and fundamental knowledge in modelling of wall filming is important for predicting the particles deposition, conversion into film thickness and related heat transfer issues. In general, the modelling of wall filming consists of several complexes and simultaneous processes such as the film flow, particle capture and particle consumption modelling. After the gas-particle phase, some of the fuel particle hits the refractory wall of the furnace, some of the particles are captured and some of the particles are rebound from the wall based on the capturing criteria in wall-particles interaction phase. In modelling of filming, gas and film flow are treated as separate single phases. So this is not a complete two-phase model but rather two single phase models attached at the film surface. The coupling of the two phases is achieved by a modified set of boundary conditions based on semi-empirical relations. It is assumed that the film thickness is very small in relation to the particle size of the gas flow which is one of the main limitations of wall filming modelling. Therefore, no adaptation of the volume grid to the wall film surface is necessary. The detailed structure of the wall filming model by combining solid-gas phase and particle-wall interaction is presented in Fig. 1.

2.1. Combustion modelling

In gas phase modelling, 3D non-steady state Eulerian partial differential conservation equations are considered for multicomponent gaseous phase. The general form of Eulerian transport equation used in the present computation is [27,28]:

$$\frac{\partial}{\partial t}(\rho\phi) + \frac{\partial}{\partial x_i}(\rho U_i \phi) = \frac{\partial}{\partial x_i}\left(\Gamma \frac{\partial \phi}{\partial x_i}\right) + S_\phi + S_{p\phi} \quad (1)$$

In particulate Phase model, discrete droplet method (DDM) [29–32] is considered. This method includes the momentum exchange, heat and mass transfer phenomena. The differential equation for a solid particle is defined as follows where the coefficient are given in [33]:

$$m_p \frac{du_{id}}{dt} = \vec{F}_{idr} + \vec{F}_{ig} + \vec{F}_{react} \quad (2)$$

$$\text{where } \vec{F}_{idr} = \frac{1}{2} \cdot \rho_g \cdot A_p \cdot C_D \cdot |u_{rel}| \cdot u_{rel} \quad (3)$$

$$\vec{F}_{ig} = V_p \cdot (\rho_p - \rho_g) \cdot g_i \quad (4)$$

$$\vec{F}_{react} = V_p \cdot \left(\frac{-m_{vp}}{dt} \right) \quad (5)$$

Eddy Breakup (EBU) model, one of the important turbulence controlled combustion model is applied for the combustion modelling. This model was first introduced by Spalding [34] and modified later by Magnussen and Hjertager [35]. This model

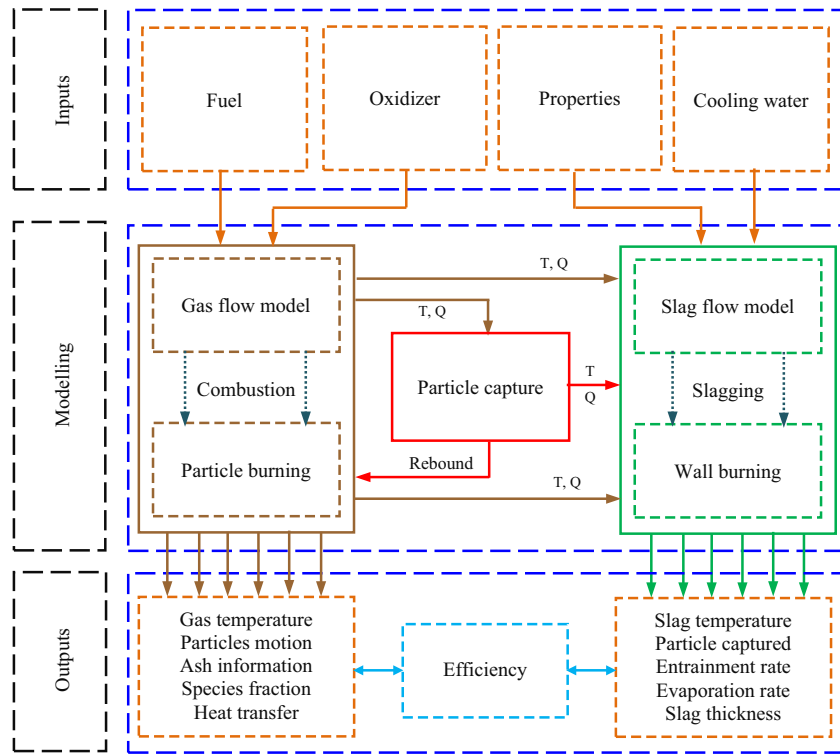


Fig. 1. Structure of the wall filming model combining gas-particle combustion phase and particle-wall interaction phase model.

determines whether, O_2 and fuel are in limiting condition and the reaction possibility. In this model, the mean reaction rate is an important parameter which is defined as [35]:

$$\bar{\rho} \dot{r}_{fu} = \frac{C_{fu}}{\tau_R} \bar{\rho} \min \left(\frac{\bar{y}_{fu}}{S}, \frac{C_{pr} \bar{y}_{pr}}{1+S} \right) \quad (6)$$

The effect of turbulence in the coal combustion gas phase is explained by Molemaker and VilÃ-Guerau de Arellano [36]. In this phase, if, y_v = volatile mass fraction, y_{ox} = oxidant mass fraction, y_c = char mass fraction, then the mass fraction of product (y_{pr}) can be calculated as:

$$y_{pr} = 1 - y_v - y_{ox} - y_c \quad (7)$$

Two very important terms in the modelling of coal combustion are devolatilisation and char oxidation. Appropriate rate constant for the process of devolatilization and char oxidation were used given in Table 1. In fuel pyrolysis simulation, the single reaction model proposed by Badzioch and Hawksley [37] is considered in this study. The volatile production rate is defined as:

$$\frac{dV}{dt} = K_v (V_f - V) \quad (8)$$

The rate constant, K_v can be defined by the Arrhenius form as:

$$K_v = A_v \exp \left(-\frac{E_v}{T_p} \right) \quad (9)$$

In this study, the char combustion is modeled with global power-law [38]. Char oxidation is the secondary phase of particle combustion after the devolatilisation. When the devolatilisation

is completed, the rest amount is char and ash. This char will react with the gases steadily [39]. In this model, diffusion of O_2 is responsible for the oxidation rate of char particle. This is treated as suitable model compared to any other models [40]. The diffusion rate of oxygen equals to $K_d(P_g - P_s)$, where K_d [41] can be defined as:

$$K_d = \frac{2.53 * 10^{-7}}{R_p} \left(\frac{T_p + T_g}{2} \right)^{0.75} \frac{P_A}{P} \quad (10)$$

Again, the rate of char oxidation per unit area is $K_c P_s$, where the value of K_c can be written as:

$$K_c = A_c \exp \left(-\frac{E_c}{T_p} \right) \quad (11)$$

Finally, the rate of the overall char reaction of a particle can also be written as follows:

$$\left(\frac{1}{K_d^{-1} + K_c^{-1}} \right) P_g 4\pi R_p^2 \frac{P}{P_A} \quad (12)$$

Radiative heat transfer is an important phenomenon in combustion modelling, considering emission [42]. Most of the proposed models for Radiative heat transfer modelling fall under the category of weighted-sum-of-gray-gases (WSGG) models [43]. In this study, the radiative heat transfer modelling is achieved considering the discrete transfer radiation method (DTRM) [44]. In this method, the blackbody emissivity is dependent on the gas temperature and the Stephan-Boltzmann constant equals to $5.67 \cdot 10^{-8} \text{ W/m}^2 \text{ K}^4$. The absorption model selected in this study is of great importance for the radiation calculation, particularly in the oxy-fuel combustion because of the higher percentage of concentration of CO_2 [45]. The gas mixture emissivity can be represented through the WSGGM as given in the following equation:

$$\varepsilon(T, x_i) = \sum_{i=1}^{I+1} \alpha_{e,i}(T) (1 - e^{-(a_{ip} + BT_c)s}) \quad (13)$$

Table 1
Kinetics data used for devolatilization and char oxidation process.

Processes	A_c	E_c	Refs.
Devolatilization	$0.2 \times 10^5 \text{ (s}^{-1}\text{)}$	$4.64 \times 10^7 \text{ J/kmol}$	[37,46]
Char oxidation	$300 \text{ kg/(m}^2 \text{ s Pa)}$	162 kJ/mol	[47,48]

The weighting factors are usually given by polynoms of order in the following form:

$$\alpha_{e,i}(T) = \sum_{j=1}^J b_{e,i,j} T^{j-1} \quad (14)$$

Accurate selection of the absorption co-efficient (for air-0.24 m⁻¹, for oxy-0.31 m⁻¹), surface discretisation (number of azimuthal division set to 8) and angular discretisation (number of polar division set to 2) is important for proper evaluation of the radiation characteristics [46,49]. More detailed information for the radiation modelling is given in [46,50–53].

For turbulence, k-ε turbulent model [54–56] is considered. In modelling coal combustion, convection and radiation heat transfer are counted during the particle and gas interaction in the furnace. The convective heat transfer is defined as:

$$Q_c = \pi D_p \lambda N_u (T_g - T_p) \quad (15)$$

The radiative heat transfer between the particle and gas is given by the following equation:

$$Q_r = \varepsilon \sigma \pi D_p^2 (T_g^4 - T_p^4) \quad (16)$$

2.2. Wall film flow model

In modelling of wall film deposition characteristics, the significant assumptions considered as lower wall film thickness, unidirectional flow, shear stress due to captured particles and wall film properties are used at wall film mean temperature. For the wall film flow, Chen [24,26] describes the three dimensional modelling that includes discrete phase and volume of fluid model for the modelling of wall film layer in horizontal and vertical furnace. The wall film flow model works based on Eulerian-Lagrangian approach which can be described by the mass, momentum and energy conservation equation. The basic governing equation for slag filming flow is the wall film thickness equation. It is a slightly modified formulation of the continuity equation, which is transformed to conservation of slag film thickness as follows:

$$\frac{\partial \delta}{\partial t} + \frac{\partial \delta u_1}{\partial x_1} + \frac{\partial \delta u_2}{\partial x_2} = \frac{1}{\rho A} (S_{mD} - S_{mV}) \quad (17)$$

One of the important features of the modelling of slag filming is the use of analytical wall film velocity profiles instead of a momentum equation. All forces acting on the slag layer resulting in shear forces which the slag film applies to the furnace refractory wall. There is a direct relation between the distribution of shear forces across the wall film layer formed and the velocity profile of the film surface flow. By applying the Boussinesq hypothesis for turbulent eddy viscosity (ε_m), the velocity profile of wall film due to applied shear forces (τ) can be written as:

$$\frac{\tau}{\rho} = (\vartheta + \varepsilon_m) \frac{\partial u}{\partial y} \quad (18)$$

The distribution of shear force across the wall film due to interfacial shear τ_i , gravity and longitudinal pressure gradient is given by:

$$\tau(y) = \left(\rho g - \frac{dp}{dx} \right) (\delta - y) + \tau_i \quad (19)$$

By applying the usual definitions for dimensionless distance from the wall

$$y^+ = \frac{yu_\tau}{\vartheta} \quad (20)$$

The dimensionless flow velocity (u^+) and friction velocity (u_τ) are as follows:

$$u^+ = \frac{u}{u_\tau} \quad (21)$$

$$u_\tau = \sqrt{\frac{\tau_w}{\rho}} \quad (22)$$

Eq. (19) can be cast into the following expression for the dimensionless velocity profile:

$$\frac{\partial u^+}{\partial y^+} = \frac{\tau/\tau_w}{1 + \varepsilon_m/\vartheta} \quad (23)$$

The wall shear force (τ_w) is the shear force (τ) at $y = 0$. For laminar flow, turbulent eddy viscosity (ε_m) equals to zero. In the case of horizontal flow, driven only by interfacial shear force ($\tau = \tau_w = -\tau_i$), the profile results to

$$u(y) = \frac{\tau_i}{\mu} y \quad (24)$$

If there is no shear force, but gravity and pressure gradient only, the profiles result to

$$u(y) = \frac{1}{\mu} \left(\rho g - \frac{dp}{dx} \right) \left(\delta y - \frac{y^2}{2} \right) \quad (25)$$

If the wall is not vertical, only the body force component parallel to the wall is used. For the case of laminar flow, the profiles of above two equations can simply be added to yield the general velocity profile [57,58]. The mean wall film velocity can be obtained by integrating over the wall film thickness (δ) as follows:

$$\bar{u}_L = \frac{\delta}{6\mu} \left[2\delta \left(\rho g - \frac{dp}{dx} \right) + 3\tau_i \right] \quad (26)$$

For the turbulent flow, in Eq. (19), it is important to define the eddy viscosity (ε_m). The eddy viscosity or turbulent viscosity can be defined as a function of wall distance y . After integrating Eq. (19), the average turbulent film velocity can be expressed as follows:

$$\bar{u}_L = \frac{49}{594} \left(\frac{\delta}{\vartheta} \right)^{4/7} \frac{\left[7\delta \left(\rho g - \frac{dp}{dx} \right) + 9\tau_i \right]}{\rho^{11/14} \left[\left(\rho g \delta - \frac{dp}{dx} \delta \right) + 9\tau_i \right]^{3/14}} \quad (27)$$

2.3. Char capture modelling

After particle introduction in the furnace, the char/ash particles hit the furnace wall, possible four major processes such as rebounding, splashing, deposition and thermal breakup can be occurred based on the thermal and hydraulic properties of the particles controlled by the capturing conditions. In most of the combustion cases, some of these heated particles are captured on the wall and some particles are rebound from the wall. Hence, determination of the amount of capturing criteria is important in modelling the wall film formation behavior in CFD. Several authors developed the particle capture sub-model to set-up particle capturing criteria for the formation of slag film on the refractory wall. Recently, Chen [24,26] used the particle capture criterion considering three major parameters, temperature of the particle (T_p), temperature of the combustor wall (T_w), and the carbon conversion of the particle (C). Based on the assumptions given in Refs. [14,59], when both the walls and the particles are sticky, the ash/char particle will be captured. If any one of the wall is not sticky, there is still a possibility for particle trapping. This trapping is determined by the Webber number having a critical value of 1.0 [60].

In the present study, the model of Kuhnke [61] is considered for settling this particle capturing behavior. The model of Kuhnke [61] is an advanced wall interaction model where wall temperature (T_w), temperature of particles (T_p), particle size and its dynamics

are important. The particles properties such as viscosity, density, thermal conductivity, specific heat, surface tension, etc. are important. This model is useful to investigate the spray/wall interaction in spray-type applications where wall temperature and the particle velocity are of importance. This model considers the mass of particles, which is deposited at the wall as well as the size and its dynamics after the impingement or entrainment. According to the model, the wall film formation strongly depends on the wall and heated particles temperature. In this model, the impact of dimensionless wall temperature (T^*) besides the impact of dimensionless velocity (V^*) is considered as the capturing criteria. The definition of dimensionless wall temperature and dimensionless particles velocity are as follows respectively.

$$T^* = \frac{T_w}{T_s} \quad (28)$$

$$V^* = \frac{(\rho_d d_d)^{\frac{3}{4}} u_d^5}{\sigma_d^{\frac{1}{2}} \mu_d^{\frac{1}{4}}} \quad (29)$$

The graphical capturing criterion is presented in Fig. 2 highlighting all the cases. From the figure, four important conditions are as follows:

- a. **Deposition:** If the value of dimensionless wall temperature, T^* is less than 1.1 and particles velocity is low, then the impacting particles are fully deposited on the wall and create a layer of wall film.
- b. **Splashing:** If the value of dimensionless wall temperature T^* is less than 1.1 but the velocity of the impacting particles is higher, the particles are divided and smaller particles are formed after the impingement. Here, a small number of particles mass are transformed to the wall film mass.
- c. **Rebound:** If the dimensionless wall temperature, T^* is greater than 1.1 and a low particle velocity is observed, a sheet layer between particles and the wall is formed which prevents a direct contact of the particles and the wall. Here, no wall film deposited.
- d. **Thermal breakup:** If the dimensionless wall temperature, T^* is greater than 1.1 and a higher particles velocity, the particles disintegrated into secondary particles and no wall film if deposited.

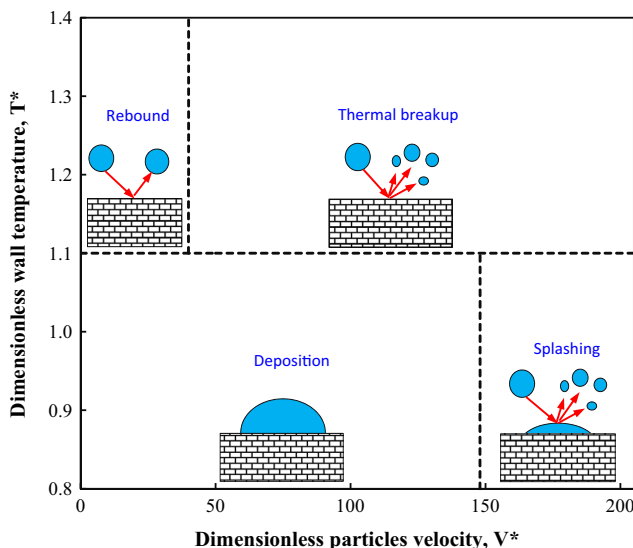


Fig. 2. Particle capturing model used for wall filming combustion [61].

2.4. Wall-film entrainment model

At high fluid velocity, the shear force at the film surface tears droplets back into the fluid flow. These droplets are generated at or near surface waves. This phenomenon is simulated within the wall-film model and described under the terms of the entrainment model. The entrainment model consists of two parts – first an entrainment mass flux is evaluated, then droplets are generated from this mass flux. The entrainment rate depends primarily on interfacial shear force, deposited film viscosity and surface tension. Droplets which become airborne are calculated by the gas-particle model. In this study, Schadel-Hanratty Model [62] was considered for entrainment modelling. The critical Weber number, specifying the onset of entrainment is defined as:

$$We_{cr,SH} = \frac{\rho_g u_{rel}^2 \delta}{\sigma} \quad (30)$$

The relative velocity u_{rel} is

$$u_{rel} = |\bar{u}_{gas} - \bar{u}_f| \quad (31)$$

Since the actual mean velocity of the gas phase is difficult to evaluate, the velocity component parallel to the wall of the cell layer from the wall was used. This is a reasonable approach for turbulent flows. When the first droplets start to entrain, the model just computes an entrainment mass flux. This entrainment rate is the amount of mass sheared off the film per unit area and unit time. This rate of atomization is described by an empirical correlation, fits to data of Schadel and Hanratty [62] which gave the model its name:

$$R_{ASH} = X_{RA} u_\tau \sqrt{\rho_g \rho_f} \cdot 10^{-3} \quad (32)$$

where

$$X_{RA} = 0.4 \cdot \ln(150 I_R \cdot We_{SH} + 1.4 \sqrt{I_R \cdot We_{SH}}) \quad (33)$$

With the roll wave intermittence factor as a function of excess film flow rate Γ_E :

$$I_R = 0.15 + 0.75 \Gamma_E, \quad I_R \leqslant 0.5 \quad (34)$$

2.5. Wall burning sub-model

After the deposition of char/ash particles on the furnace wall and formation of thin wall film layer, a slow wall burning process may occur if the required oxygen level is available. The wall burning process is dependent on the deposition level of char particles. A detailed analysis about the wall burning process are given in Refs. [15,18]. Basically, wall burning is a slower char combustion process because of the slower diffusion of oxygen (O_2) on the external surface of the deposited particles [21,22,24,26]. Similar to the char combustion in particulate phase modelling, deposited slag can be combusted using global power-law [38]. This is treated as suitable model compared to any other models [40]. When the char/ash par-

Table 2
Slag properties used for modelling.

Properties	Values	Unit	Refs.
Temperature of critical viscosity	1680	K	[16]
Dynamic viscosity	1–20	Pa s	[63]
Density	2780	kg/m ³	[64,65]
Thermal conductivity	1.73–1.80	W/m K	[64,65]
Surface tension	430×10^{-3}	N/m	[64,65]
Specific heat cp	1.3825	kJ/kg K	[64,65]
Latent heat	355×10^3	J/kg	[66]
Slag emissivity	0.83		[64,65]
Thermal diffusivity	4.5×10^{-7}	m ² /s	[16]

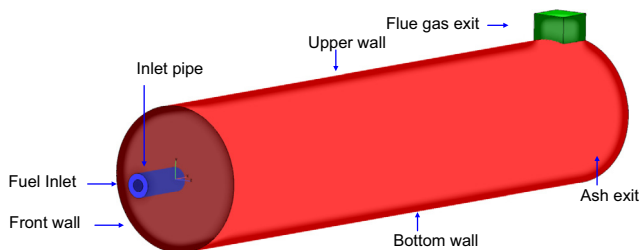


Fig. 3. Schematic diagram of the Physical model used for wall filming combustion.

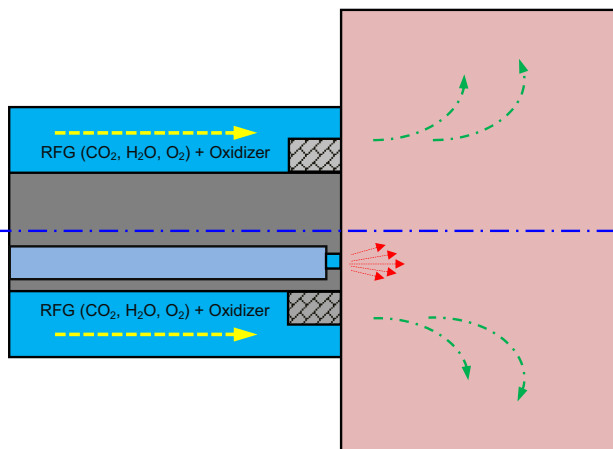


Fig. 4. A simplified design of the burner used for wall filming modelling.

Table 3

Fuel properties and particle data used for the modelling.

Proximate analysis (wt%, ar)		Ultimate analysis (wt%, ar)	
Moisture content	6.40	Carbon, C	82.10
Ash content	7.00	Hydrogen, H	05.40
Volatile matter	33.1	Nitrogen, N	01.40
Fixed carbon	53.5	Sulphur, S	00.60
HHV, MJ/kg	29.15	Oxygen, O	11.46

ticles are deposited as wall film, this slag film may react with the surrounding gases steadily [39]. But the rate of deposited wall film burning will be significantly lower than the particles oxidation due to slower diffusion of O_2 .

2.6. Slag properties

Selection of appropriate slag properties is important for modelling of wall film formation behavior. Determination of slag properties such as viscosity, density, specific heat, surface tension and thermal conductivity are dependent on constituents of the fuel particles which can be measured by using X-ray fluorescence (XRF) method [22]. The chemical compositions of the slag vary due to variation of coal slag origination. The temperature of critical viscosity is one of the most important properties which can be defined as the temperature where a transition between the liquid

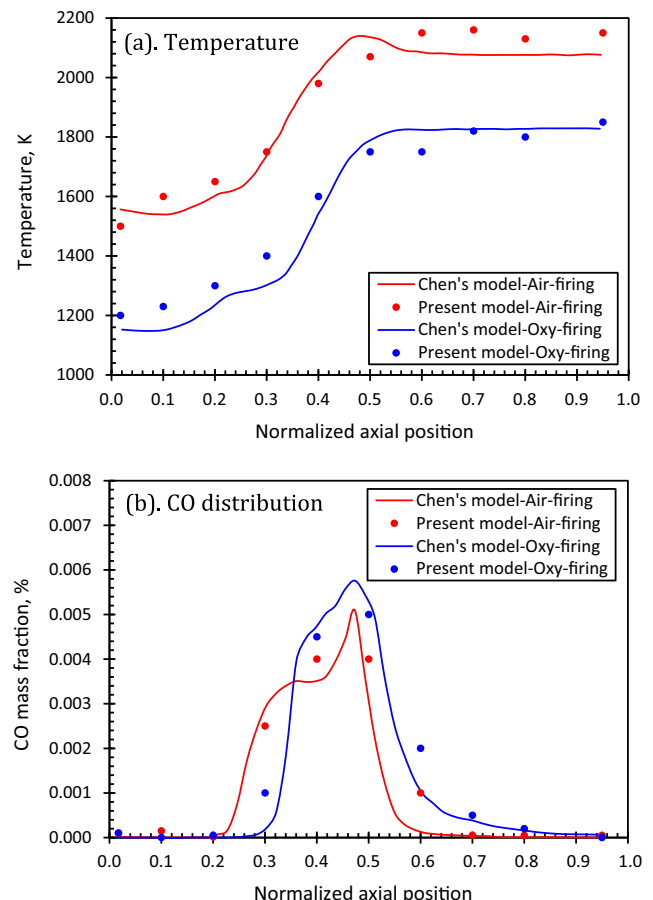


Fig. 5. Comparison of (a) temperature and (b) species (CO) prediction between Chen's model [26] and present model under air and oxy-fuel conditions.

and the plastic flow is occurred. It is challenging to predict due to abrupt changes between the liquid and solid wall film layers interface. Due to lack of data from the experimental studies on the ash properties, sometimes properties are predicted based on correlations [64,67–70]. The slag properties data used in the present study is given in Table 2. A user-defined subroutine was coupled with the CFD code for incorporating the slag properties such as temperature of critical viscosity, dynamic viscosity, density, surface tension, specific heat capacity, latent heat of evaporation, slag emissivity and thermal diffusivity.

3. Validation and results

3.1. Physical model

In this study, the physical model of 5 MWth coal water slurry scaled combustor given in Refs. [71,72] was considered. The schematic diagram of the computational domain showing important components is presented in Fig. 3. It is seen that a burner is mounted at the center of the front end of the combustor for facilitating the

Table 4

Boundary parameters for different coal-water slurry combustion cases.

Cases	Flow conditions			Oxidizer compositions				Coal supply		
	Q (kg/s)	T (K)	P (bar)	O ₂ (%)	N ₂ (%)	CO ₂ (%)	H ₂ O (%)	T (K)	P (bar)	Q (kg/s)
Air	1.12	305	4.0	0.21	0.79	0.00	0.00	62	15	0.1
Oxy	1.13	305	4.0	0.22	0.037	0.36	0.38	62	15	0.1

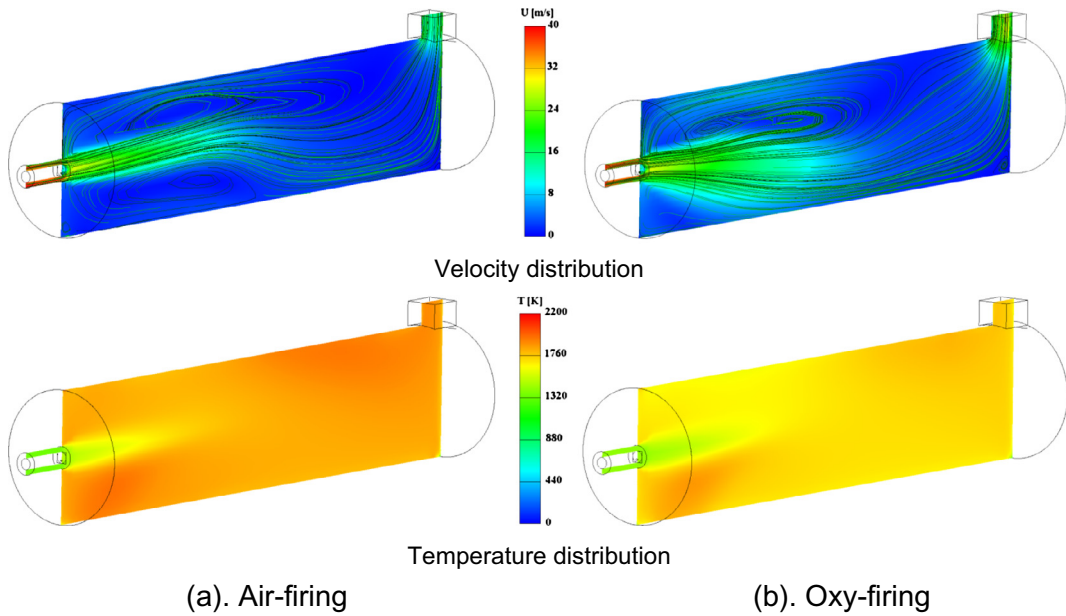


Fig. 6. Velocity (m/s) and gas temperature (K) distribution for (a) air-firing, (b) oxy-firing case.

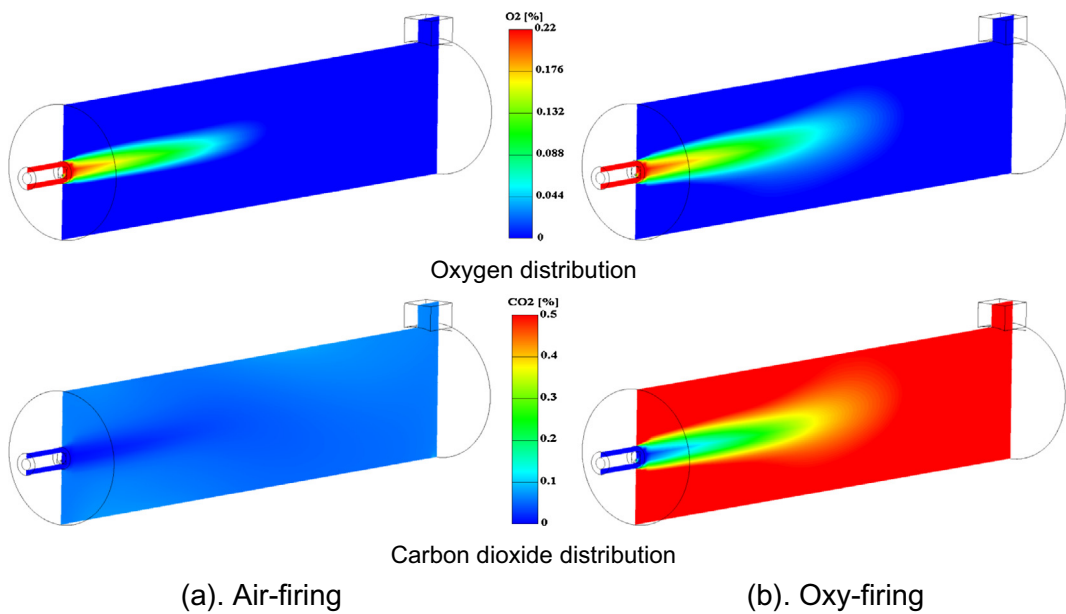


Fig. 7. Oxygen (O_2) and carbon dioxide (CO_2) mass fraction (%) distribution for different cases.

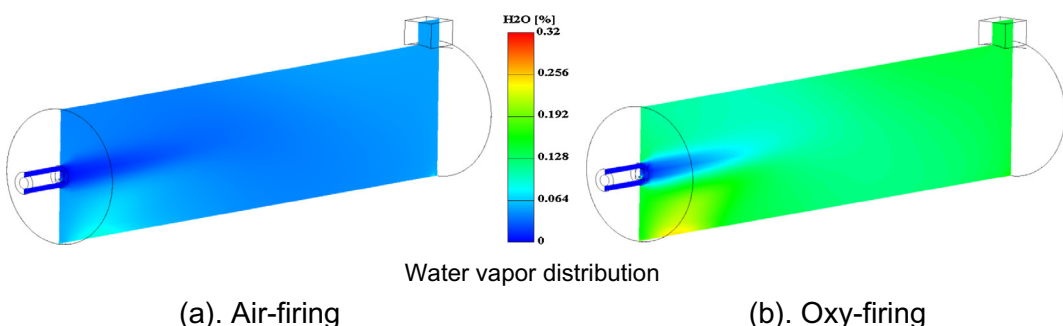


Fig. 8. Water vapor (H_2O) mass fraction (%) distribution for different cases.

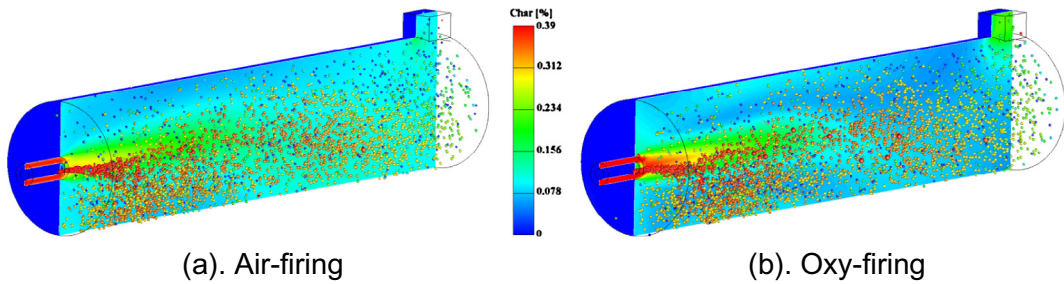


Fig. 9. Char mass fraction distribution for (a) air-firing and (b) oxy-firing cases.

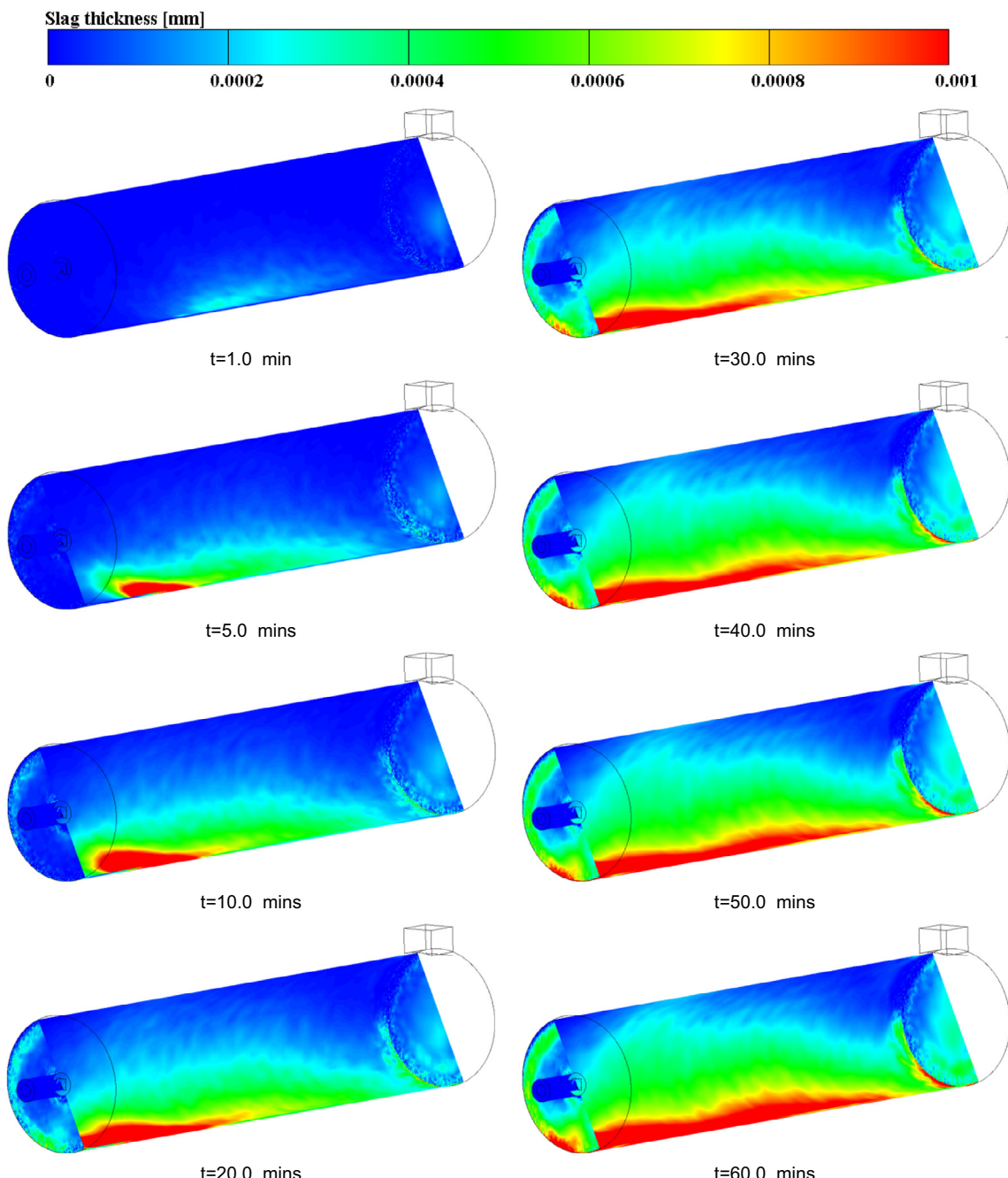


Fig. 10. The wall film thickness build-up in the transient calculation for air-firing.

coal/oxidizer flow into the reaction zone. As the fuel is mixed with water, an atomizer is attached with the burner design. A simplified design of the furnace is given in Fig. 4. The position of the atomizer is at a small distance down from the burner center. The oxidant flow consists of recycled flue gas such as O₂, N₂, CO₂, H₂O are stabilized by a constant swirling flow to the furnace. The fuel properties used for this study were given in Table 3. For coal, the particles mean diameter of 200 µm was used for both air-firing and oxy-fuel cases.

3.2. Fuel properties, cases and boundary values

The different operating conditions were characterized by air-firing and oxy-firing cases. The compositions of O₂, N₂, CO₂ and H₂O for both the cases are presented in Table 4. The operating conditions used in this study were based on the optimized and scaled

down to a 3 MWth operating condition in Ref. [72]. For all cases, a constant temperature and high pressure were maintained for oxidizer and atomizer flows. The coal-water slurry mass flow rate was maintained at 0.1 (kg/s) for all the cases simulated. For stability and better mixing of the flow, a constant swirl number of 0.8 was used. For different section of the furnace wall, no-slip boundary conditions were assumed and constant wall temperature and emissivity were used for the furnace. At the flue gas and molten ash exit of the furnace, zero gradient for all the variables were assumed.

3.3. Validation of the combustion model

It is seen from the literature that a significant amount of published plant data for the combustion of various types of solid fuels was available for the combustion models used in CFD. Available

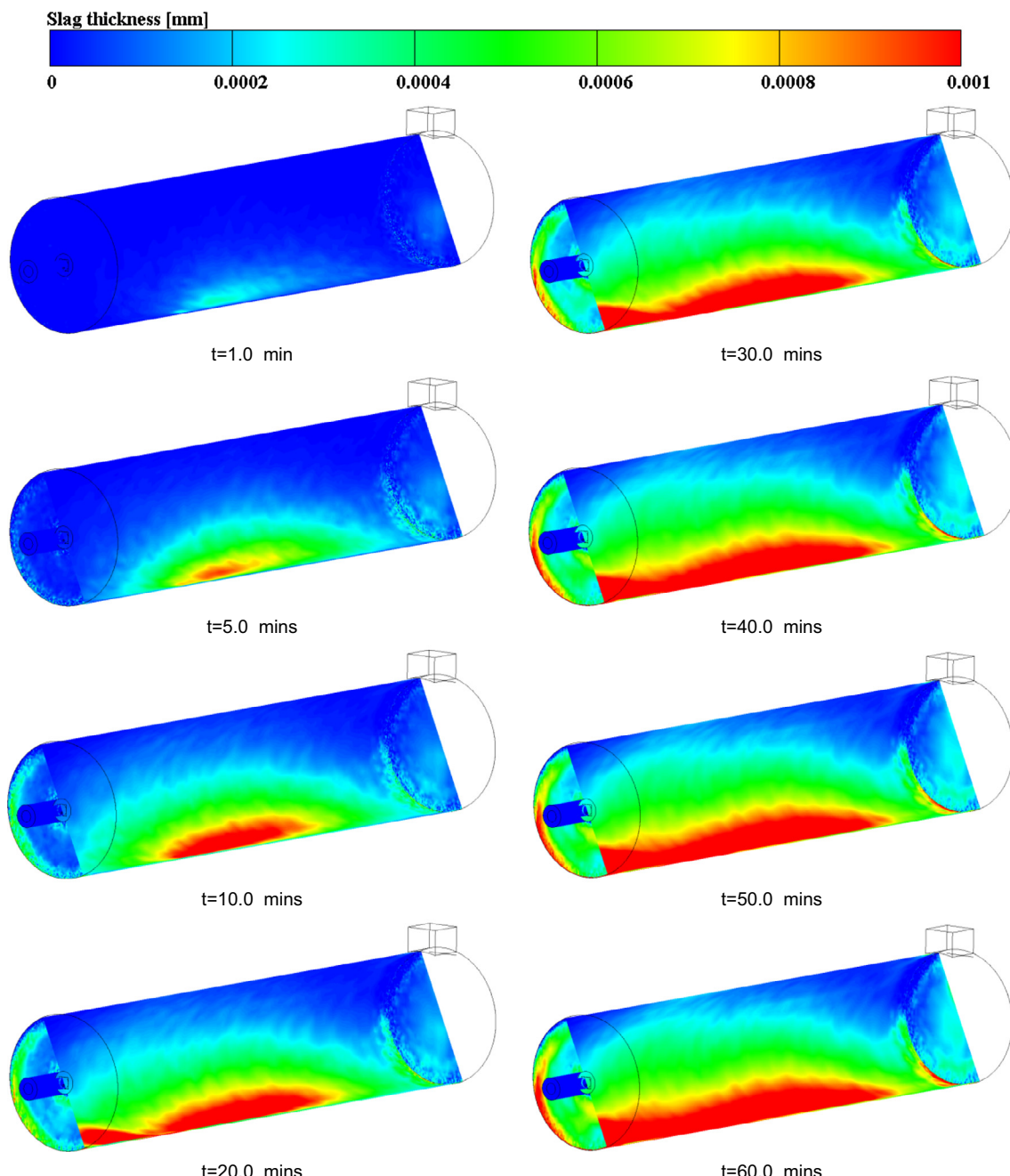


Fig. 11. The wall film thickness build-up in the transient calculation for oxy-firing.

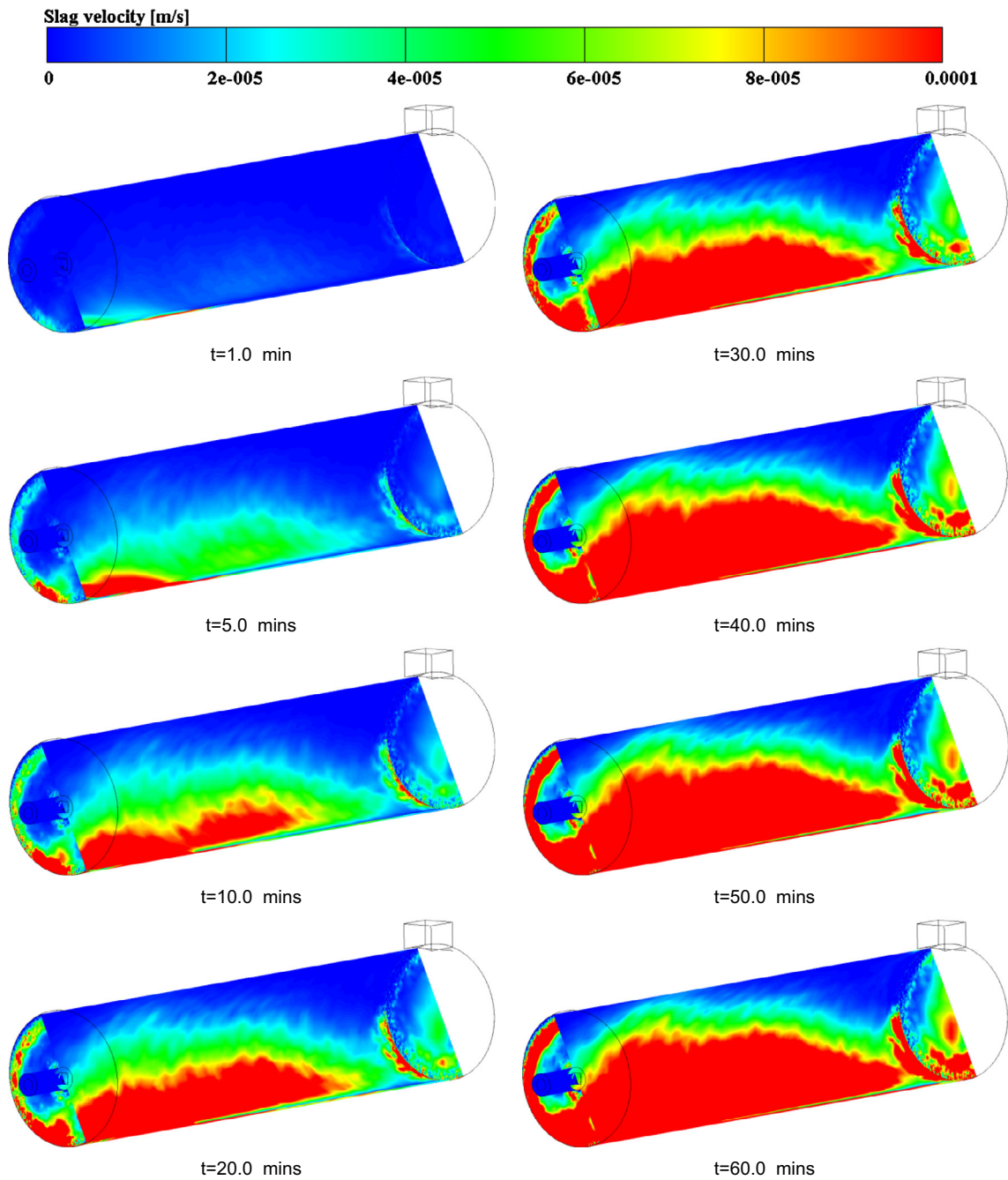


Fig. 12. The wall film surface velocity (m/s) in the transient calculation for air-firing.

combustion models in CFD are quite generic models and applicable to a wide range of combustion problems. But little information is available for the wall film formation phenomenon. Hence, the validation of the developed wall filming model is carried out against the CFD data of coal-water slurry combustion in Chen's model [26]. Fig. 5 shows the comparison of axial temperature distribution and CO mass fraction distribution under air and oxy-firing conditions between the Chen model [26] and the present model. Though presence of some discrepancies in the modelling was observed while validating against the CFD data, but overall a reasonable data range was predicted. It is seen that the temperature increases along the axis of the furnace. Similar findings have been observed in the study of Chen [26]. It was also found that the wall film layer spread over the bottom wall of the furnace due to flows of the side

wall and also gravity. The deposited wall film thickness over the wall was found in the range of 0–1 mm. This is mainly due to the transient build-up of ash/char particle deposition. Thus, the CFD faithfully reproduced the wall film deposition characteristics for the selected combustion case.

3.4. Effect of temperature and flow distributions

In this study, a comprehensive investigation on the thermal and wall filming characteristics of coal-water slurry combustion has been investigated considering air and oxy-fuel combustion environment. Results are presented based on flow dynamics, temperature distribution and species distributions, etc. Fig. 6 presents the flow distribution of the oxidizer and gas temperature distributions

for both the cases. The velocity distribution along the reactor length is presented and no significant variation is observed as can be seen from the flow condition given in [Table 4](#). This is due to similar swirling flow (swirl number = 0.8) considered for both the cases. Comparatively lower recirculation is visualized in oxy-firing case which is responsible for lower residence time leading to lower mixing of the fuel with oxidizer. This lower residence time lead to lower flame temperature in oxy-firing case. The visualization of temperature shows that peak value is found too far from the burner exit in both cases. This is due to injection of coal-water slurry particles near the burner and reaction area. The fuel/oxidizer components having higher fraction of H₂O in slurry compositions compared to coal/air flow lead to delayed ignition in the oxy-firing case. The peak temperature for air and oxy-firing cases were found 2085 and 1905 K respectively.

3.5. Effect of species concentration during wall filming

[Fig. 7](#) presents the distribution of the oxidizer (O₂) and associated CO₂ concentration contours for air-firing and oxy-firing cases. These two parameters are closely related to each other. Prediction of mass fraction (kg/kg) distribution of CO₂ and O₂ are important phenomena in oxy-fuel cases which contribute to the heat transfer, flame temperature characteristics. It is seen from [Table 4](#) that slightly higher O₂ is supplied in oxy-firing case compared to air-firing case. With the presence of higher O₂ in oxy-case, an increase in gas temperature is expected. But a significant decrease in the gas temperature is observed. This can be explained on the basis of higher amount of H₂O and CO₂ fraction having higher heat capacity in the latter case. This dampens the characteristics of better oxidizing capability of O₂ in oxy-firing case.

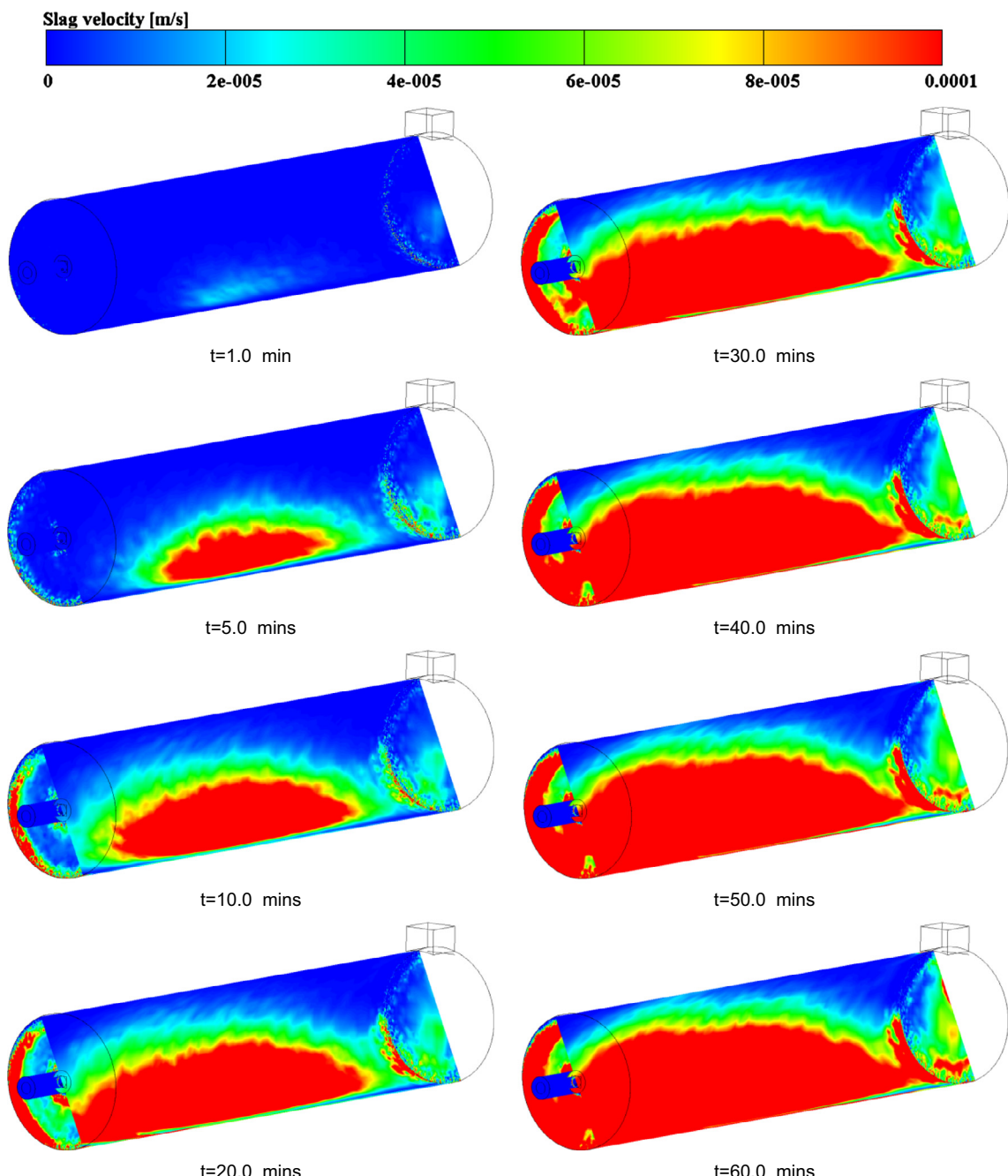


Fig. 13. The wall film surface velocity (m/s) in the transient calculation for oxy-firing.

The water vapor (H_2O) mass fraction (kg/kg) distribution in the direction of furnace length for all the cases considered in this study are presented in Fig. 8. The figure represents the water vapor mass fraction (kg/kg) distribution for all the cases. It is seen from the figure that highest value of the water fraction is found in the furnace bottom. The coal-water slurry particles are injected into the furnace which is further interacted with the furnace wall. Comparatively higher water vapor mass fraction is predicted in oxy-firing cases. This causes higher heat sink and lower temperature rise in oxy-firing case. As seen in Fig. 5(b), the increase in the CO concentrations of the latter case was found. This is due to the lower gas temperature of the combustion cases and hence lower reaction rate of the CO oxidation. The gas temperature levels in the air-fired case affected the CO concentrations in the flame regions. The peak CO values expected in the flame region were convoyed by the lowest CO_2 values. The generation of CO mass fraction can be demonstrated by the mechanism of Boudouard reaction given in [46].

Fig. 9 characterizes the mass fraction of char particles in the furnace. Particle tracking mechanism represents that char particles are moving in the lower part of the furnace due to forces acting on it. The heated particles are burned in the later part of the furnace. The rapid reduction of oxygen concentration in the furnace negatively affected the oxidation of the residual char in the remaining part of the furnace. That's why comparatively higher order of char fraction is predicted in oxy-firing case due lower reduction of O_2 as presented previously.

3.6. Variation of wall film thickness and flow characteristics

The main objective of this modelling was to develop an understanding of how the particles interact with the wall in the furnace. In order to achieve this, a number of sub-models were incorporated assuming different limitation under different operating conditions. The wall film formation modelling was developed by combining solid fuel combustion and particles-wall interaction scheme coupled in a commercial CFD framework.

Figs. 10 and 11 show the wall film thickness build-up in the transient calculation for air-firing and oxy-firing cases respectively. It is seen from these figures that the deposited layer of wall film spreads over the furnace walls. Compared to other sides, significant fractions of layer were deposited in the lower wall. It is seen that the thickness of the deposited wall film layer in the lower portion of the furnace was approximately 0–1.0 mm. This wall film layer builds up due to deposition of the char particle on the furnace wall. When molten char/ash particles hit the furnace wall, based on the capturing criteria, these particles are captured and deposited on the wall. Due to particle motion and the gravity effect, this newly formed molten wall film layer is driven in the downwards direction. If the operating temperature is below the fusion temperature, a solid wall film layer may be formed in between the molten wall film layer and the wall. Compared to air-firing case, slightly higher fraction of wall film layer is deposited in the oxy-firing case. It can also be seen that the wall film is thicker at the lower part of the furnace due to the wall film accumulation along its path; this is due to the lower char oxidation rate in oxy-firing case. It would be useful to understand the dynamics of how the transient molten wall film flows after the deposition on the furnace wall as the measurement of deposited layer thickness and flow behavior in a conventional way is difficult. Hence, this model provides a pattern of formation of wall film layer and its flow characteristics to apply the developed model to a real life furnace by CFD.

Figs. 12 and 13 show the wall film surface velocity on the furnace wall for air-firing and oxy-firing respectively. As the furnace is horizontally placed at an inclination of 1.5° , so the molten wall film moves towards the end of the furnace with time. When the

particles deposited on the side wall, these wall film flows down to the bottom of the furnace. The flow of the molten wall film occurs due to gravity and momentum of the particle deposition. The wall film possessed high viscosity and surface tension properties as can be seen from Table 2, hence the wall film velocity is significantly lower than the gas velocity. It is found that the maximum wall film velocity is approximately 0.0001 m/s.

4. Conclusion

This study represents the development of wall filming model in industrial furnace. AVL Fire 2009.2 coupled with user-defined subroutines were incorporated for combining coal combustion with wall film formation mechanisms. This study was performed considering in two stages. Validation of the model was achieved by comparing temperature and species (CO) distribution along the axis of the furnace. The wall film thickness deposited on the furnace wall was found in the range of 0.0–1.0 mm which was reasonably in good agreement with the available data. The wall film surface velocity was found approximately 0.1 mm/s. Transient build-up of the wall film thickness with wall film surface velocity were illustrated considering air and oxy-firing cases. Comparatively higher fraction of wall film layer was predicted due to incomplete combustion of the char component. Also the effects of species mass fraction, flame temperature and flow distribution in different oxidizing environments were presented. Overall, this study will provide a guideline for predicting wall film formation in real life furnace.

References

- [1] T. Wall et al., Coal ash fusion temperatures—new characterization techniques, and implications for slagging and fouling, *Prog. Energy Combust. Sci.* 24 (4) (1998) 345–353.
- [2] A.A. Bhuiyan, J. Naser, Modeling of slagging in industrial furnace: a comprehensive review, *Proc. Eng.* 105 (2015) 512–519.
- [3] J.M. Beér, Combustion technology developments in power generation in response to environmental challenges, *Prog. Energy Combust. Sci.* 26 (4) (2000) 301–327.
- [4] J. Fen, *Principles and Calculations of Boilers*, second ed., Science Press, Beijing, 1992.
- [5] H. Haykiri-Acma, S. Yaman, S. Kucukbayrak, Co-combustion of low rank coal/waste biomass blends using dry air or oxygen, *Appl. Therm. Eng.* 50 (1) (2013) 251–259.
- [6] M. Habermehl et al., Experimental and numerical investigations on a swirl oxyco flame, *Appl. Therm. Eng.* 49 (2012) 161–169.
- [7] L. Chen, S.Z. Yong, A.F. Ghoniem, Oxy-fuel combustion of pulverized coal: characterization, fundamentals, stabilization and CFD modeling, *Prog. Energy Combust. Sci.* 38 (2) (2012) 156–214.
- [8] N. Nikolopoulos et al., Numerical investigation of the oxy-fuel combustion in large scale boilers adopting the ECO-Scrub technology, *Fuel* 90 (1) (2011) 198–214.
- [9] C.G. Yin et al., Use of numerical modeling in design for co-firing biomass in wall-fired burners, *Chem. Eng. Sci.* 59 (16) (2004) 3281–3292.
- [10] A.A. Bhuiyan, J. Naser, Modelling of slag deposition and flow characteristics of coal combustion under oxy-firing condition in a 550 MW tangentially fired furnace, *Appl. Therm. Eng.* 106 (2016) 221–235.
- [11] Y. Niu, H. Tan, S.E. Hui, Ash-related issues during biomass combustion: alkali-induced slagging, silicate melt-induced slagging (ash fusion), agglomeration, corrosion, ash utilization, and related countermeasures, *Prog. Energy Combust. Sci.* 52 (2016) 1–61.
- [12] J. Ni et al., Molten slag flow and phase transformation behaviors in a slagging entrained-flow coal gasifier, *Ind. Eng. Chem. Res.* 49 (23) (2010) 12302–12310.
- [13] F. Montagnaro, P. Salatino, Analysis of char–slag interaction and near-wall particle segregation in entrained-flow gasification of coal, *Combust. Flame* 157 (5) (2010) 874–883.
- [14] S. Li, Y. Wu, K.J. Whitty, Ash deposition behavior during char–slag transition under simulated gasification conditions, *Energy Fuels* 24 (3) (2010) 1868–1876.
- [15] X. Wang et al., Modeling of a coal-fired slagging combustor: development of a slag submodel, *Combust. Flame* 149 (3) (2007) 249–260.
- [16] M. Seggiani, Modelling and simulation of time varying slag flow in a Prenflo entrained-flow gasifier, *Fuel* 77 (14) (1998) 1611–1621.
- [17] W. Reid, P. Cohen, Factors affecting the thickness of coal-ash slag on furnace-wall tubes, *Trans. ASME* 66 (1944) 685–690.

- [18] X. Wang et al., The deposition and burning characteristics during slagging co-firing coal and wood: modeling and numerical simulation, *Combust. Sci. Technol.* 181 (5) (2009) 710–728.
- [19] N. Wood, Mass transfer of particles and acid vapor to cooled surfaces, *J. Inst. Energy* 54 (419) (1981) 76–93.
- [20] P.M. Walsh, A.F. Sarofim, J.M. Beer, Fouling of convection heat exchangers by lignitic coal ash, *Energy Fuels* 6 (6) (1992) 709–715.
- [21] S.Z. Yong, A. Ghoniem, Modeling the slag layer in solid fuel gasification and combustion—two-way coupling with CFD, *Fuel* 97 (2012) 457–466.
- [22] S.Z. Yong, M. Gazzino, A. Ghoniem, Modeling the slag layer in solid fuel gasification and combustion—formulation and sensitivity analysis, *Fuel* 92 (1) (2012) 162–170.
- [23] M. Bockelie, et al., CFD Modeling for Entrained Flow Gasifiers in Vision 21 Systems, 2003.
- [24] L. Chen, S.Z. Yong, A.F. Ghoniem, Modeling the slag behavior in three dimensional CFD simulation of a vertically-oriented oxy-coal combustor, *Fuel Process. Technol.* 112 (2013) 106–117.
- [25] S. Liu, Y. Hao, Numerical study on slag flow in an entrained-flow gasifier, in: ASME 2007 International Mechanical Engineering Congress and Exposition, American Society of Mechanical Engineers, 2007.
- [26] L. Chen, A.F. Ghoniem, Development of a three-dimensional computational slag flow model for coal combustion and gasification, *Fuel* 113 (2013) 357–366.
- [27] A.A. Bhuiyan, J. Naser, Numerical modelling of oxy fuel combustion, the effect of radiative and convective heat transfer and burnout, *Fuel* 139 (2015) 268–284.
- [28] A.A. Bhuiyan, J. Naser, Computational modelling of co-firing of biomass with coal under oxy-fuel condition in a small scale furnace, *Fuel* 143 (2015) 455–466.
- [29] A.A. Bhuiyan, J. Naser, Thermal characterization of coal/staw combustion under air/oxy-fuel conditions in a swirl-stabilized furnace: a CFD modelling, *Appl. Therm. Eng.* 93 (2016) 639–651.
- [30] A.A. Bhuiyan, J. Naser, Numerical modeling of biomass Co-combustion with pulverized coal in a small scale furnace, *Proc. Eng.* 105 (2015) 504–511.
- [31] A.A. Bhuiyan, J. Naser, CFD modelling of co-firing of biomass with coal under oxy-fuel combustion in a large scale power plant, *Fuel* 159 (2015) 150–168.
- [32] A.A. Bhuiyan, J. Naser, Effect of recycled ratio on heat transfer performance of coal combustion in a 0.5 MWth combustion test facility, in: 19th Australasian Fluid Mechanics Conference Melbourne, Australia, 2014.
- [33] L.N.Z. Schiller, A drag coefficient correlation, *Vet. Dtsch. Ing.* 77 (1933) 318–320.
- [34] D.B. Spalding, Mixing and chemical reaction in steady confined turbulent flames, *Symp. (Int.) Combust.* 13 (1) (1971) 649–657.
- [35] B.F. Magnussen, B.H. Hjertager, On mathematical modeling of turbulent combustion with special emphasis on soot formation and combustion, *Symp. (Int.) Combust.* 16 (1) (1977) 719–729.
- [36] M.J. Molenaar, J. Vilà-Guerau de Arellano, Control of chemical reactions by convective turbulence in the boundary layer, *J. Atmos. Sci.* 55 (1998) 568–579.
- [37] S. Badzioch, P.G. Hawksley, Kinetics of thermal decomposition of pulverized coal particles, *Ind. Eng. Chem. Process Des. Dev.* 9 (4) (1970) 521–530.
- [38] M.A. Field, D.W. Gill, B.B. Morgan, P.G.W. Hawksley, Combustion of Pulverized Coal, The British Coal Utilization Research Association, Leatherhead, 1967, pp. 186–210.
- [39] I.W. Smith, in: Proceedings of the 19th Symposium (International) on Combustion. The Combustion Institute, Pennsylvania, 1983, pp. 1045–1066.
- [40] G.H. Gronhovd et al., Low-Rank Coal Technology: Lignite and Subbituminous, 1982.
- [41] M. Baum, P. Street, Predicting the combustion behaviour of coal particles, *Combust. Sci. Technol.* 3 (5) (1971) 231–243.
- [42] H. Abdul-Sater, G. Krishnamoorthy, An assessment of radiation modeling strategies in simulations of laminar to transitional, oxy-methane, diffusion flames, *Appl. Therm. Eng.* 61 (2) (2013) 507–518.
- [43] P. Nakod et al., A comparative evaluation of gray and non-gray radiation modeling strategies in oxy-coal combustion simulations, *Appl. Therm. Eng.* 54 (2) (2013) 422–432.
- [44] F.C. Lockwood, N.G. Shah, A new radiation solution method for incorporation in general combustion prediction procedures, *Symp. (Int.) Combust.* 18 (1) (1981) 1405–1414.
- [45] P. Edge et al., LES modelling of air and oxy-fuel pulverised coal combustion—impact on flame properties, *Proc. Combust. Inst.* 33 (2) (2011) 2709–2716.
- [46] A.H. Al-Abbas, J. Naser, D. Dodds, CFD modelling of air-fired and oxy-fuel combustion of lignite in a 100 KW furnace, *Fuel* 90 (5) (2011) 1778–1795.
- [47] Y. Wu et al., Three-dimensional simulation for an entrained flow coal slurry gasifier, *Energy Fuels* 24 (2) (2010) 1156–1163.
- [48] B. Brown et al., Measurement and prediction of entrained-flow gasification processes, *AIChE J.* 34 (3) (1988) 435–446.
- [49] T. Nozaki et al., Analysis of the flame formed during oxidation of pulverized coal by an O₂/CO₂ mixture, *Energy* 22 (2) (1997) 199–205.
- [50] A.H. Al-Abbas, J. Naser, Effect of chemical reaction mechanisms and NO_x modeling on air-fired and oxy-fuel combustion of lignite in a 100-kW furnace, *Energy Fuels* 26 (6) (2012) 3329–3348.
- [51] A.H. Al-Abbas, J. Naser, D. Dodds, CFD modelling of air-fired and oxy-fuel combustion in a large-scale furnace at Loy Yang A brown coal power station, *Fuel* 102 (2012) 646–665.
- [52] J. Hart, A.H. Al-Abbas, J. Naser, Numerical investigation of pyrolysis of a Loy Yang coal in a lab-scale furnace at elevated pressures, *Heat Mass Transf.* 49 (12) (2013) 1725–1732.
- [53] A.H. Al-Abbas et al., Numerical modelling of oxy-fuel combustion in a full-scale tangentially-fired pulverised coal boiler, *Proc. Eng.* 56 (2013) 375–380.
- [54] A.A. Bhuiyan, M.R. Amin, A.K.M.S. Islam, Three-dimensional performance analysis of plain fin tube heat exchangers in transitional regime, *Appl. Therm. Eng.* 50 (1) (2013) 445–454.
- [55] A. Bhuiyan, A. Islam, M. Amin, Numerical study of 3D thermal and hydraulic characteristics of wavy fin-and-tube heat exchanger, *Front. Heat Mass Transf.* 3 (3) (2012).
- [56] A.A. Bhuiyan, A.S. Islam, M.R. Amin, Numerical prediction of laminar characteristics of fluid flow and heat transfer in finned-tube heat exchangers, *Innov. Syst. Des. Eng.* 2 (6) (2011) 1–12.
- [57] D. Ullmann, L. Prandtl, K. Oswatitsch, K. Wieghardt, Führer durch die Strömungslehre, 9, verb. u. erw. Auflage, Braunschweig/Wiesbaden, Friedrich Vieweg & Sohn 1990. XIII, 648 S, 458 Bilder, DM 148,—. 108–108, ZAMM-J. Appl. Math. Mech./Z. Angew. Math. Mech. 73(2) (1993). ISBN 3-528-28209-6.
- [58] S. Yih, Modeling heat and mass transfer in wavy and turbulent falling liquid films, *Wärme Stoff.* 21 (6) (1987) 373–381.
- [59] G.H. Richards, P.N. Slater, J.N. Harb, Simulation of ash deposit growth in a pulverized coal-fired pilot scale reactor, *Energy Fuels* 7 (6) (1993) 774–781.
- [60] J. Senda et al., Modeling of diesel spray impinging on flat wall, *JSME Int. J. Ser. B* 39 (4) (1996) 859–866.
- [61] D. Kuhnke, Spray Wall Interaction Modelling by Dimensionless Data Analysis PhD thesis, Technische Universität Darmstadt, 2004.
- [62] S. Schadel, T. Hanratty, Interpretation of atomization rates of the liquid film in gas-liquid annular flow, *Int. J. Multiphase Flow* 15 (6) (1989) 893–900.
- [63] S. Vargas, F.J. Frandsen, K. Dam-Johansen, Rheological properties of high-temperature melts of coal ashes and other silicates, *Prog. Energy Combust. Sci.* 27 (3) (2001) 237–429.
- [64] K.C. Mills, J.M. Rhine, The measurement and estimation of the physical properties of slags formed during coal gasification: 2. Properties relevant to heat transfer, *Fuel* 68 (7) (1989) 904–910.
- [65] K.C. Mills, J.M. Rhine, The measurement and estimation of the physical properties of slags formed during coal gasification: 1. Properties relevant to fluid flow, *Fuel* 68 (2) (1989) 193–200.
- [66] J.M. Weiss, The latent heat of vaporization of coal-tar oils, *Ind. Eng. Chem.* 14 (1) (1922), pp. 72–72.
- [67] J. Watt, F. Fereday, Flow properties of slags formed from ashes of British coals. 1. Viscosity of homogeneous liquid slags in relation to slag composition, *J. Inst. Fuel* 42 (338) (1969) 99.
- [68] J.W. Nowok, J.P. Hurley, D.C. Stanley, Local structure of a lignitic coal ash slag and its effect on viscosity, *Energy Fuels* 7 (6) (1993) 1135–1140.
- [69] J. Patterson et al., Evaluation of the Slag Flow Characterization of Australian Coals in Slagging Gasifiers, Research Report, 2001.
- [70] S. Vargas, F. Frandsen, K. Dam-Johansen, Rheological properties of high-temperature melts of coal ashes and other silicates, *Prog. Energy Combust. Sci.* 27 (3) (2001) 237–429.
- [71] J. Hong et al., Analysis of oxy-fuel combustion power cycle utilizing a pressurized coal combustor, *Energy* 34 (9) (2009) 1332–1340.
- [72] L. Chen, M. Gazzino, A.F. Ghoniem, Characteristics of pressurized oxy-coal combustion under increasing swirl number, in: Proceedings of the 35th International Technical Conference on Clean Coal & Fuel Systems, 2010.